GeoScienceWorld
Lithosphere
Volume 2022, Article ID 7223019, 12 pages
https://doi.org/10.2113/2022/7223019

Lithosphere

Research Article

Genesis Mechanism of Deep Carbonate Reservoir in Jizhong Depression

Qingzhuang Miao,[1,2,3] Guiling Wang,[2,3] Shihua Qi,[1] Linxiao Xing,[2,3,4] Hailiang Xin,[5] and Xiaoni Zhou[2]

[1]*State Key Laboratory of Biogeology and Environmental Geology, China University of Geosciences, Wuhan 430074, China*
[2]*Institute of Hydrogeology and Environmental Geology, Chinese Academy of Geological Sciences, Shijiazhuang 050061, China*
[3]*Technology Innovation Center of Geothermal & Hot Dry Rock Exploration and development, Ministry of National Resources, Shijiazhuang 050061, China*
[4]*School of Environmental Studies, China University of Geosciences, Wuhan 430074, China*
[5]*Geophysical Exploration Center, China Earthquake Administration, Zhengzhou 450002, China*

Correspondence should be addressed to Guiling Wang; ihegwagnguiling@sina.com

Received 16 July 2022; Revised 21 September 2022; Accepted 17 November 2022; Published 7 December 2022

Academic Editor: Shuo Zhang

The occurrence condition of geothermal resources in Jizhong depression is good for development, but the thermal genetic mechanism of thermal reservoir has been lack of systematic and theoretical research, which leads to large number of failure cases in the process of geothermal well location. In this paper, the thermal genetic mechanism of thermal reservoir in Jizhong depression is explored in the aspects of heat source, heat source channel, and thermophysical structure by means of core thermophysical property test, magnetotelluric sounding, and natural seismic P wave velocity imaging. According to the study, the heat of deep carbonate reservoir in Jizhong depression mainly comes from the deep mantle. Heat from the mantle enters deep thermal reservoir in the form of thermal conduction and thermal convection which flows through deep faults such as Niudong-Hexiwu fault. Cenozoic sandstone and mudstone caprock whose thermal conductivities are low is more than 1000 meters, which is favorable for heat storage. In comparison, the thermal conductivity of deep carbonate thermal reservoir is much higher than that of sandstone and mudstone. Therefore, differences in thermal conductivity and thermal convection from deep faults are the reasons why the heat reservoir temperature in the uplift area is higher than that in the subdepression area at the same depth.

1. Introduction

Geothermal energy is a renewable clean energy with large reserves, wide distribution, and easy utilization. So, it is a competitive new energy [1]. The distributions of geothermal resources in China, which are mostly distributed in large sedimentary basins and mountains with good geothermal display, are obviously regular and regional. Among them, there are good geothermal resources [2], relatively high exploration and development, and mature technologies in Jizhong depression [3]. It is one of the regions with better geothermal resource development and utilization in China [4, 5].

Some achievements have been made in the geothermal research in Jizhong depression. Chen Moxiang studied the longitudinal and plane distribution characteristics of geothermal gradient in Niutuozhen uplift area of Jizhong depression according to the measured temperature of boreholes [6]. Some researchers discussed the distributions of heat flow and paleo-geothermal evolution history of Cenozoic strata in Raoyang sag and Langgu sag of Jizhong depression based on the systematic temperature data and rock thermal conductivity data [7]. Some researchers studied the distributions of geothermal gradient or terrestrial heat flow in Jizhong depression and believed that the plane distribution was related to the relief of basement topography [8, 9]. In terms of deep structure, the massive lithospheric thinning, crustal deformation, earthquake, and magmatic activity caused by the destruction of the North China Craton

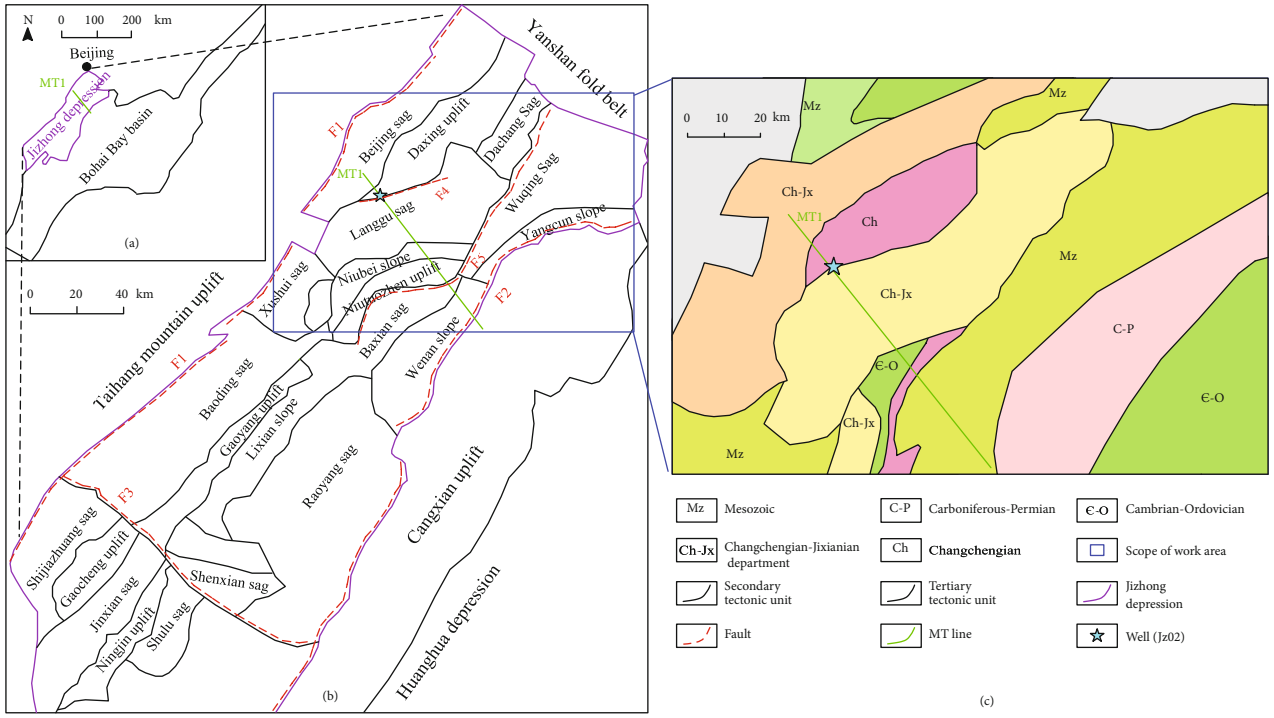

FIGURE 1: Structure and geology of sectional Jizhong depression. (F1: Taihang Mountain piedmont fault, F2: Xianxian fault, F3: Hengshui fault, F4: Daxing fault, F5: Niudong-Hexiwu fault).

also created good conditions for the deep heat to enter the shallow strata and form geothermal resources [10]. Some of the major faults cut through the aluminum silicate layer and penetrated deep into the magnesium silicate layer or the upper mantle. And they played an important role in controlling the upward conduction of deep heat and the formation of geothermal resources [11].

This paper conducts thermal property tests on core samples and analyzes the characteristics of radiogenic heat rate and thermal conductivity of the main lithologies in the study area. And genesis mechanism of geothermal resource is discussed combining magnetotellurics and seismic tomography. The results can not only provide theoretical support and scientific basis for the evaluation and rational development of geothermal resource in Jizhong depression but also enrich the theoretical understanding of the genesis mechanism of geothermal resource in sedimentary basin in China.

2. Regional Geological Setting

2.1. Regional Structure Characteristics. Jizhong depression located in the north of North China Plain is a depression in the west of Bohai Bay basin, bordering on Yanshan fold belt in the north, Xingheng Uplift in the south, Taihang Mountain uplift in the west, and Cangxian uplift in the east, with an overall NE-SW trend. It can be divided into 12 sags, such as Raoyang sag, Baxian sag, and Langgu sag, and 6 uplifts (Figure 1). It is composed of continental sedimentary rocks of Eocene to Pliocene with mixture of volcanic rocks, with few outcrops, and covered by the Quaternary system. The main body of the unit is a basin that has been continuously faulted since the Eocene.

There are three kinds of faults in Jizhong depression: NNE, NE, and SW. NNE trending faults are the most developed ones in this area, which are large in scale, long in extension, steeper in dip angle, and are arranged in right-side. The fault activity was still strong in Cenozoic, which controlled Oligocene sedimentation. The NE faults are consistent with the axial direction of the basement fold, and most of them are distributed in the axial part of the fold with a gentle dip angle. The SW fault is small in scale. The main faults can be seen in Figure 1. The thermal fields in Jizhong depression are controlled by these faults, which are widely distributed in the whole region [12].

2.2. Regional Geological Characteristics. From Proterozoic to the end of Triassic, Jizhong depression it developed a set of relatively stable carbonate rock and clastic rock deposits, which transferred from marine facies to paralic facies and then to continental facies with stable deposition and wide distribution [13]. Tectonic movement and magmatic activity are relatively gentle, mainly oscillatory movement. During the Jurassic period and its later period, a series of continental clastic rocks were formed, with strong tectonic and magmatic activities and mainly faulted deposits.

Jizhong depression is a Mesozoic-Cenozoic sedimentary depression developed on the basement of North China paleo-platform, which is characterized by the development of Paleogene and Neogene.

Archaean: forming the base of the North China platform.

Proterozoic: a set of marine strata deposited on the base of the North China platform after the Luliang Movement. From the bottom up, the strata include the Changchengian

system, Jixianian system, and Qingbaikouian system, which are mainly carbonate rocks interlaced with sandstones, shales, and chert bands and masses. Among them, Wumishan Formation is the most developed stratum, with the maximum drilling thickness of 2200 m in the study area [14].

Lower Paleozoic: it is a set of marine sediments in the stable subsidence period of the region after the Neoproterozoic. There are the Cambrian strata and Ordovician strata in the area, and the lithology is mainly carbonate rock, which is widely distributed in the area.

Upper Paleozoic: Triassic strata are lack in the study area, and the Carboniferous-Permian strata are mainly developed.

Cenozoic: during the late Mesozoic Yanshan movement, a series of NEE trending faults were produced, which acted together with the early EW trending faults to cut and separate the blocks, and established the structural pattern of north-south zoning and east-west zoning in Jizhong depression. Since the Paleogene, the fault activity has become more intense, resulting in the vertical differentiation of the bedrock blocks. The uplifted side of the block was subjected to strong denudation, while the descending side received rapid accumulation. Early Paleogene ultimately overlapped on the bedrock, forming an obvious angular unconformability. The thickness of the Quaternary system is 260~490 m. The general trend is that the buried hill area in the northwest is thin, and the depression area in the southeast is gradually thicker.

3. Research Methods and Test Results

3.1. Core Thermophysical Property Test. The rock density, U element content, Th element content, K element content, and thermal conductivity of 50 samples collected from borehole named JZ02 (Figure 1) were tested. The test principle of rock density is Archimedes principle, and the test method is apparent density method. The instrument is XF-220SD high-precision digital solid-liquid denser, with an accuracy of 0.0001 g/cm^3. The radioactive elements were determined by tetra-acid digestion, and the contents of U and Th were detected by ICP-MS with an error ± 5% confined and a detection limit of 0.01 ppm. K content was detected by ICP-OES, the error was within ±5%, and the detection limit was wt.0.001%. The thermal conductivity was tested by improved method of transient planar heat source with the instrument named TCi Thermal Conductivity Analyzer produced by C-Therm firm in Canada. The test accuracy and repeatability were better than 5% and 1%. The density test needs sample to be in blocks without broken, and the thermal conductivity test needs the core section to be smooth. Because of the requirements for the test of samples, 44 samples of density and 39 samples of thermal conductivity were tested (Table 1).

Heat generation rate of rock can be calculated according to the measured density and the content of U, Th, and K:

$$A\left[\mu\mathrm{W}\cdot\mathrm{m}^{-3}\right] = 10^{-5}\times\rho\left[\mathrm{kg}\cdot\mathrm{m}^{-3}\right] \times\left(9.52\,C_{\mathrm{U}}[\mathrm{ppm}] + 2.56\times C_{\mathrm{Th}}[\mathrm{ppm}] + 3.48\times C_{\mathrm{K}}[\%]\right), \quad (1)$$

where A is heat generation rate of rocks (μW·m^3), C_{U} and C_{Th} are the content of U and Th in rocks (ppm), C_{K} is the K content (wt%), ρ is the density of rocks (kg·m^{-3}).

3.2. Magnetotelluric Sounding. The five-component instrument named V8-6R/RUX-3E produced by Phoenix Company in Canada was used for magnetotelluric data acquisition, with the frequency range of 320~0.0005 Hz, 40 effective frequencies and the detection depth of 6000~10000 m. The profile, whose length was about 58 km, passed through several geological tectonic units [15]. And its point distance was 400~1000 m. A total of 61 measuring points were recorded; the profile was about 120 km. In order to meet the periodic length of impedance phase data, the recording time of all measuring points was more than 12 hours, and the data was collected at night. The 2D magnetotelluric processing, inversion interpretation, and imaging software system (MTSoft 2D 2.4) were used for data preprocessing. And NLCG inversion was performed [16].

According to the magnetotelluric result (Figure 2), electrical structure in Jizhong depression is obviously heterogeneous, and there are three main electrical layers in the longitudinal direction: the surface layer shows low resistivity, which is inferred to be the Quaternary layer; the middle layer also shows low resistivity (lower than the surface resistivity), which is inferred to be the interbedded sandstone and mudstone of Neogene and Paleogene; the deep layer shows high resistivity, which is inferred to be limestone or carbonate of Mesozoic or Paleozoic. According to the topographic relief of high resistivity in the profile, the shallow buried area with high resistivity is raised area, while the deep buried area with high resistivity is sag area.

3.3. Analysis of Crustal P Wave Velocity Structure. The crustal velocity structure represents the physical properties of deep crust. Seismic tomography technology has been widely used in the acquisition of the velocity structure of the earth's interior and has achieved lots of results [17]. Probe for crustal velocity structure of North China has been carried out since the 1980s, using body wave travel time tomography of natural seismic [18] and surface wave tomography [19], and artificial seismic exploration technology [20, 21], obtained a large number of results, providing a scientific reference for analysis of the relationship between deep structure and deep heat storage in the study area.

Different seismological methods mentioned above have different sensitivities and resolutions to geological structures [22]. Artificial seismic sounding characterized by high detection accuracy is the primary method for detecting the fine structure of crust and mantle [23]. After collecting and sorting 42 wide-angle reflection/refraction profiles of 2D artificial seismic in the study area and adjacent areas since 1976 [24], the velocity structure and interface structure of the profile were gridded. A fine 3D P wave velocity structure named HBCrust1.0 (Figure 3) of the crust in the central and eastern North China Craton was constructed using Kriging interpolation method. For the velocity structure, the depth and velocity of the interface are meshed according to the grid spacing of 5.0 km in transverse direction and 2.0 km in depth

Table 1: Thermophysical parameter statistics of borehole lithology.

Sample number	Lithology	Depth (m)	Density (kg·m^{-3})	U (μg/g)	Th (μg/g)	K (μg/g)	Heat generation (μW·m^{3})	Thermal conduction (W/mK)
JZ02-1	Sand interbedded clay	200.00-201.30	/	1.82	11.92	1.74	/	1.879
JZ02-2	Mud clamps gravel	415.26-416.26	2.1068	0.90	6.76	1.80	0.6773	2.138
JZ02-3	Basalt	639.41-642.11	2.6959	0.11	0.91	0.17	0.1061	1.986
JZ02-4	Mudstone	860.40-862.40	2.2459	1.36	8.24	2.03	0.9247	2.250
JZ02-5-1	Mudstone	1080.28-1083.80	/	1.44	8.62	1.68	/	2.456
JZ02-5-2	Mudstone	1080.28-1083.80	/	0.93	5.63	2.22	/	/
JZ02-6	Sandstone	1251.00-1252.20	2.2301	1.25	7.11	1.90	0.8178	2.337
JZ02-7-1	Mudstone	1450.00-1454.00	2.1934	1.57	8.55	2.15	0.9728	2.036
JZ02-7-2	Sandstone	1450.00-1454.00	/	8.15	7.83	1.69	/	2.290
JZ02-8	Sandstone	1648.00-1652.50	2.718	0.61	0.53	0.058	0.1999	/
JZ02-9	Sandstone	1723.32-1726.32	2.7405	0.67	0.41	0.029	0.2057	3.592
JZ02-10	Dolomite	1798.50-1799.00	2.8338	0.30	0.53	0.095	0.1285	/
JZ02-11	Dolomite	1808.59-1809.99	2.8699	0.56	0.65	0.12	0.2124	4.259
JZ02-12	Dolomite	1911.74-1919.74	2.8135	0.71	2.83	0.80	0.4721	5.413
JZ02-13	Dolomite	1961.37-1962.37	2.8563	0.20	0.59	0.12	0.1099	4.782
JZ02-14	Dolomite	2064.44-2067.94	2.701	1.64	8.22	2.92	1.2633	4.713
JZ02-15	Mudstone	2093.02-2099.02	2.5481	1.57	13.07	7.26	1.8779	1.598
JZ02-16	Gneiss	2177.16-2178.86	2.6419	1.85	20.45	4.75	2.2855	3.461
JZ02-17	Gneiss	2254.15-2258.15	2.7114	0.38	16.73	3.80	1.6177	/
JZ02-18	Gneiss	2258.15-2263.15	2.6964	0.20	1.43	4.29	0.5526	2.500
JZ02-19	Gneiss	2367.85-237145	2.7274	0.13	1.43	4.13	0.5257	2.097
JZ02-20	Gneiss	2452-2456.4	2.8122	0.29	2.96	1.85	0.4724	2.488
JZ02-20-1	Gneiss	2452-2456.4	2.8122	0.44	2.64	1.81	0.4840	/
Time 2-1	Sand interbedded clay	200.00-201.30	2.4783	0.70	3.45	1.63	0.5254	2.263
Time3-1	Basalt	639.41-642.11	2.7215	0.13	0.82	0.16	0.1060	/
Time4-1	Mudstone	860.40-862.40	2.1378	1.73	8.69	2.37	1.0032	2.119
Time5-1	Mudstone	1080.28-1083.80	2.5886	1.28	7.80	1.84	0.9975	/
Time5-2	Sandstone	1080.28-1083.80	/	1.09	6.68	2.56	/	/
Time6-1	Sandstone	1251.00-1252.20	2.2617	1.76	8.13	1.86	0.9965	2.267
Time7-1	Mudstone	1450.00-1454.00	2.5906	1.80	7.35	2.02	1.1146	2.171
Time7-2	Sandstone	1450.00-1454.00	2.1275	1.07	6.13	1.93	0.6926	2.149
Time8-1	Sandstone	1648.00-1652.50	2.6221	0.34	0.33	0.036	0.1099	2.913
Time9-1	Sandstone	1723.32-1726.32	2.7203	0.88	0.32	0.022	0.2527	/
Time11-1	Dolomite	1808.59-1809.99	2.8120	1.08	3.96	1.49	0.7191	5.045
Time12-2	Dolomite	1911.74-1919.74	2.7836	0.52	1.94	0.49	0.3236	2.701

Table 1: Continued.

Sample number	Lithology	Depth (m)	Density (kg·m^{-3})	U (μg/g)	Th (μg/g)	K (μg/g)	Heat generation (μW·m^{3})	Thermal conduction (W/mK)
Time12-3	Dolomite	1911.74-1919.74	2.7892	0.38	1.70	0.47	0.2691	4.627
Time13-1	Dolomite	1961.37-1962.37	2.7752	0.10	0.36	0.048	0.0566	5.146
Time14-1	Dolomite	2064.44-2067.94	2.7060	2.10	8.97	3.45	1.4861	4.615
Time15-1	Mudstone	2093.02-2099.02	2.5963	1.03	9.86	9.22	1.7440	/
Time15-3	Mudstone	2093.02-2099.02	2.5793	1.57	11.39	8.56	1.9057	1.446
Time15-4	Gneiss	2177.16-2178.86	/	1.57	11.89	8.66	/	/
Time16-1	Gneiss	2254.15-2258.5	2.7118	0.53	9.04	3.86	1.1289	2.386
Time17-1	Gneiss	2259.15-2263.15	2.6566	0.25	39.92	3.82	3.1311	2.502
Time18-1	Gneiss	2367.85-2371.45	2.6534	0.20	2.53	3.97	0.5902	3.036
Time20-2	Gneiss	2452.00-2456.40	2.7476	0.37	1.83	2.98	0.5107	2.327
Time16	Gneiss	/	2.7138	2.00	53.88	4.48	4.6827	3.242
Time17	Dolomite	/	2.6878	0.49	13.37	3.89	1.4100	2.804
Time18	Gneiss	/	2.6359	0.59	0.84	4.47	0.6141	2.795
Time19	Gneiss	/	2.7574	0.21	0.67	3.03	0.3926	2.377
Time20	Gneiss	/	2.7427	1.09	1.22	3.04	0.6613	2.356

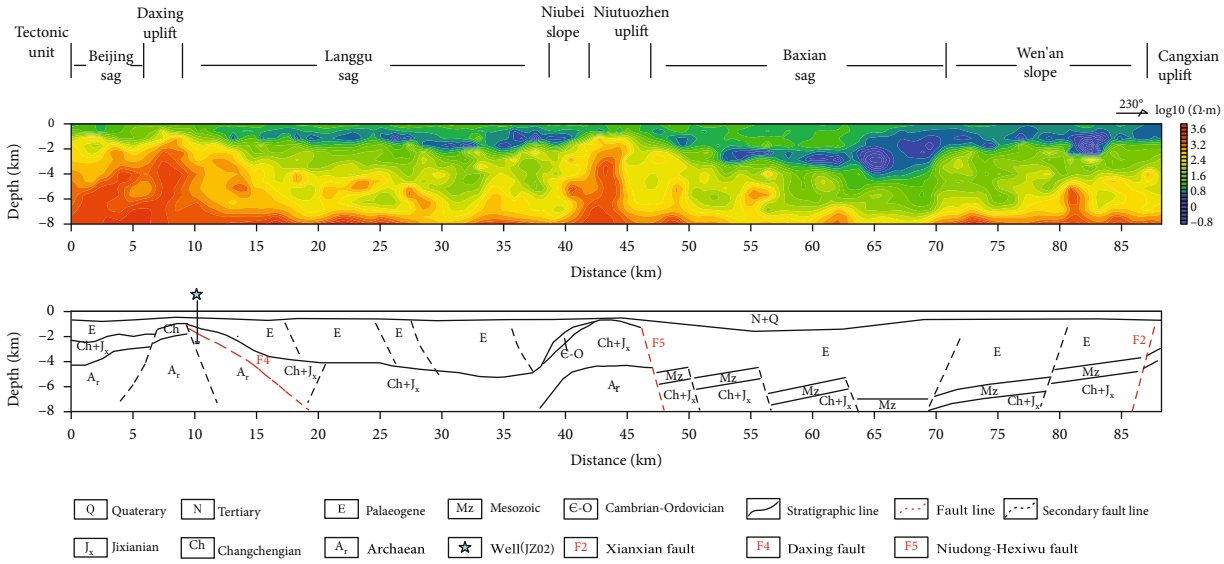

Figure 2: 2D inversion section and geological interpretation of magnetotelluric soundings.

direction (the grid spacing of more than 10 km in depth direction is 1.0 km). The model can distinguish velocity anomalies greater than 0.05 km/s, and the accuracy of Moho depth is about ±1.0 km. Figure 3 shows the velocity distributions of HBCrust1.0 at five different depths from 2 km in the shallow crust to 26 km in the lower crust, as well as the depth of Moho.

The velocities at 2 km and 5 km show the velocity structure of sedimentary cover in the study area. The thickness and velocity structure of sedimentary cover in the eastern and central parts of the study area are obviously different. The eastern depression basin is mainly composed of Cenozoic and Mesozoic deposits, and the sedimentary cover velocity is 2.0~5.0 km/s. The interphase distribution of high and low velocity areas corresponded well with the depressions and uplift of the geological structure. The depression area and the uplift area are distributed in NNE-NE direction, with obvious east-west division and differences between north and south, reflecting the tectonic characteristics of North China Basin caused by the NW tensile stress field since Cenozoic.

The velocities at 10 km and 20 km reflect the velocity structure of the middle and upper crust. It shows that the velocity structure has great lateral variation, but does not correspond to the geological structure as well as the sedimentary cover. The existence of low-velocity layer is an important geological phenomenon of this layer. The depth of 26 km is located in the lower crust, where the lateral velocity structure has great changes, and the P wave velocity generally ranges from 6.3 to 6.6 km/s. The distribution of high and low velocity is relatively scattered in North China Plain. Figure 3(f) shows the depths of Moho interface in the study area. It shows that the depth of Moho interface in North China basin is 31-32 km. The depth variation of Moho interface shows that Taihang Mountain fault is the boundary, and the Moho interface obviously sinks gradually from east to west.

4. Analysis and Discussion

The research on the genesis of geothermal resources mainly includes four aspects: heat source, heat source channel, heat reservoir, and caprock. At present, the heat sources of geothermal research in China are more recognized as radioactive heat generation [25], magmatic capsule [26], fault communication [27], and other heat sources. In the following, mechanism of thermal storage in Jizhong depression will be discussed in four aspects: heat source, heat source channel, caprock, and reservoir.

4.1. Radioactive Heat Generation. The study of radioactive heat generation rate of rocks is one of the main elements of the study of the genesis of geothermal systems [28]. Here, radioactive heat generation rate of different lithologic strata is statistically calculated. The results of the heat generation rate of borehole rock are listed in Table 2. Figure 4 shows the radiogenic rates at different depths. The results are shown as follows:

(1) Sandstone and dolomitic limestone have relatively low radioactive heat generation rates, with an average of 0.43 μW/m^3 and 0.48 μW/m^3, which are consistent with the results of previous studies that there were low content of heat generation elements for sandstone and dolomitic limestone [25, 29]

(2) The radioactive heat generation rate of gneiss is relatively high with an average of 1.20 μW/m^3, which is lower than the average of 2.30 μW/m^3 of gneiss in other parts of China [30]. The maximum value reached 4.68 μW/m^3 at the depth of 2100 m

There are two parts of heat flow in the sedimentary basin [31]: one part is crustal heat flow, which comes from radioactive decay in crust such as U, Th, and K; the other part is mantle heat flow that comes from the deep mantle.

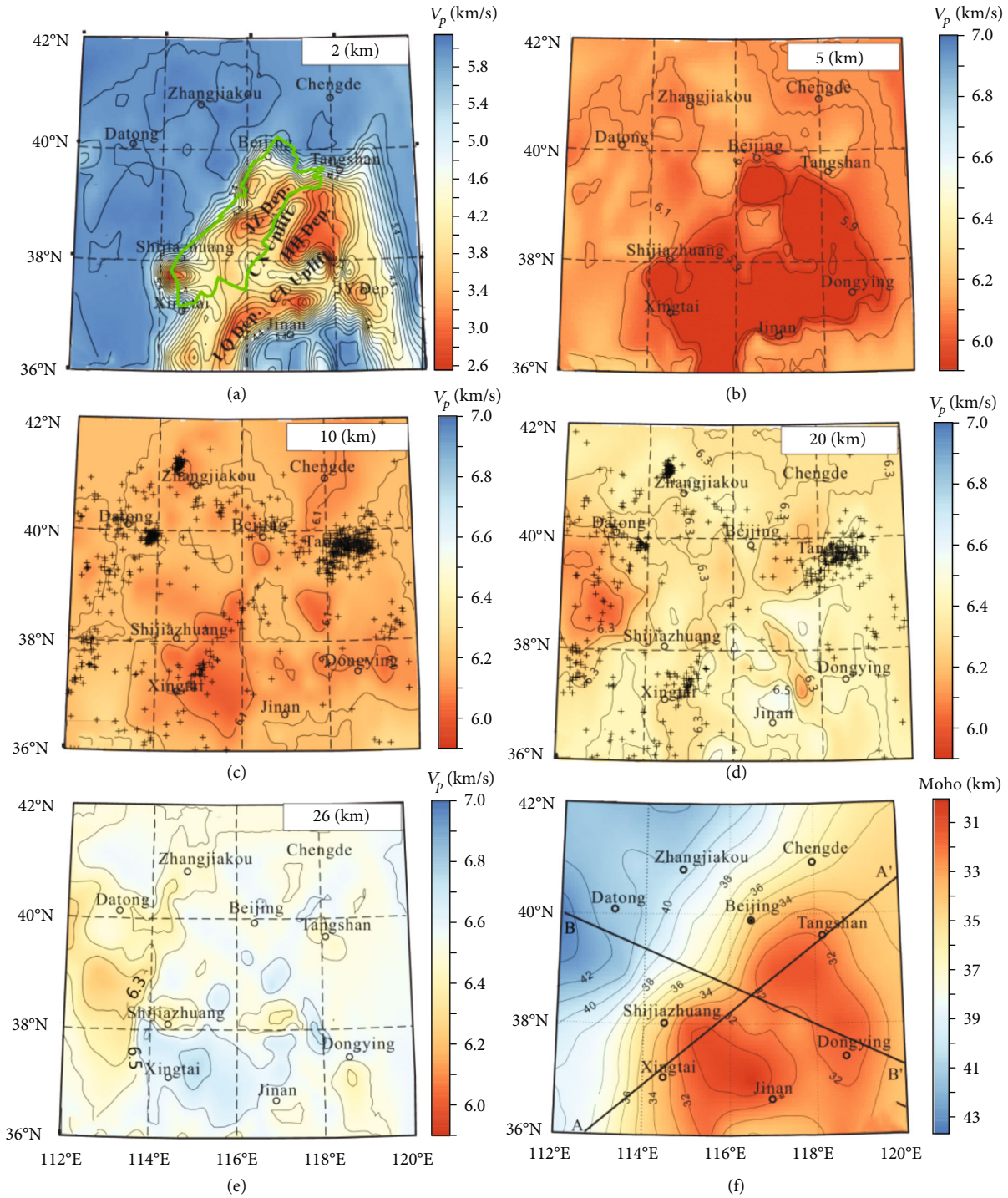

FIGURE 3: P wave velocity distribution at different depth of the crust (a–e) and depth distribution of Moho plane (f) (modified from Duan et al. [24]). JZ Dep., Jizhong depression. Depth is shown at the top-right corner of each map. Black crosses in (c) and (d) are focus depths between 5-15 km and 15-25 km, respectively, projected at corresponding depths. BB′ in (f) are the position of the velocity structure profile in Figure 5.

Lithospheric thermal structure refers to the distribution ratio of heat flow between crust and mantle and its fabric relationship in a region. In this paper, a back-stripping method is used to calculate heat flow in sedimentary basin based on surface heat flow, heat generation rate, and crustal thickness [32]. The calculation formula is as follows:

$$q_m = q_s - q_c = q_s - \sum A_i D_i. \quad (2)$$

In this formula, q_c, q_m, and q_s are heat flow of crust, mantle and surface (mW/m^2), A_i is the heat generation rate of layer i (μW/m^3), and D_i is the thickness of layer i.

Table 2: Statistics of heat generation rate of rock.

Lithology	Sample quantity	Heat generation rate ($\mu W/m^3$)	Average value ($\mu W/m^3$)
Mudstone	9	0.68-1.86	1.25
Sandstone	9	0.11-1.00	0.43
Dolomite	9	0.06-1.49	0.48
Gneiss	14	0.39-4.68	1.20

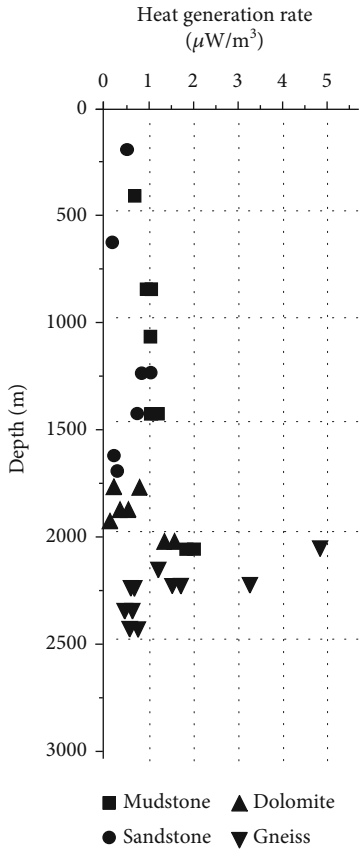

Figure 4: Statistical graph of heat generation rate of rock in depths.

Lithologic structure in the crust is complex. In order to estimate thermal model of study area, reasonable assumptions and simplifications can be put forward in the calculation (Table 3), as follows:

(1) If two lithologic depth range is not continuous and unable to determine boundary range in depth, taking the distance between them half as boundary depth, in turn, has carried on the generalized to formation lithology in the calculation process

(2) After ignoring the extremely high value of heat generation rate, the background value of heat generation rate was calculated to be 0.75 $\mu W/m^3$, and the strata calculated in crust were divided into upper crust, middle crust, and lower crust [33]

(3) The value of heat flow in the study area is 79.1-90 mW/m^2 [34]

According to the statistical results in Table 3, the crustal heat flow is about 20.45 mW/m^2; the heat flow value of the surface is about 79.1-90 mW/m^2; the mantle heat flow is about 8.7-69.6 mW/m^2. And the crustal heat flow contribution rate is 22.72-29.85%. It can be seen that the contribution rate of heat flow generated by crustal heat generation is less than 30%, and most of the heat source comes from the deep mantle. We call the study area is a "cold crust and hot mantle" lithospheric thermal structure.

4.2. Magma Capsule. Magma in crust is the important heat source for shallow heat reservoirs [26]. In this paper, whether magma is existent is studied indirectly by means of seismic wave velocity. Figure 5 shows vertical sections of P wave velocity along the NE-trending BB′ profile (positions of profiles are seen in Figure 3(f)). The BB′ section passes through Taihang Mount uplift area and Jizhong depression from the northwest to the southeast. The profile shows that the overall lateral variation of crustal velocity changes greatly. Taking Taihang mountain fault as the boundary, the deepest part of the Moho interface of Taihang mountain reaches 42 km, while the depth of the North China Plain is about 32~35 km, showing a state of uplift as a whole, in which the study area named Jizhong depression is located.

In the profile, there is an obvious low-velocity body distribution at the depth of 10 to 15 km in Jizhong depression, and its P wave velocity is 5.0~6.0 km/s, while the P wave velocity at the same depth is generally 6.0~6.3 km/s in the transverse section. There are some disputes about the genesis of the low velocity and high conductivity layer in crust of the North China Plain. The main viewpoints are as follows: (1) water-bearing fluid hypothesis [35]; (2) magma melting hypothesis [36]; (3) Shear zone hypothesis [37]. In addition, there is also a view that the low-velocity and high-conductivity layer is caused by the superposition of multiple action [38, 39]. For the magma melting hypothesis, the existence of low velocity and high conductivity layer is equivalent to the existence of heat source, which provides heat for the shallow heat reservoir. In a word, the Moho interface of the North China Plain is uplifting on the whole, and the low velocity layer of the middle and lower crust may be the encroachment of the mantle magma on the bottom of the crust.

In the profile, it shows that there is no low-velocity anomaly from the low-velocity body down to the mantle, indicating that there is no low-velocity magma body from the deep. The low-velocity body is located in the upper part of the middle crust, where Taihang Mountain piedmont fault is transformed into a low-angle ductile shear zone. There are also some near-horizontal reflective layers, which are the horizontal demolition zone and ductile shear zone formed during the fracture trap extension. And semibrittle deformation makes the structure of the rock composition nonuniform, the lattice oriented, and many microfractures [40]. These have been confirmed in ultradeep drilling [41]. Therefore, the low velocity layer in the upper middle crust of the Jizhong depression is due to the influence of the ductile shear zone formed by the Taihang Mountain piedmont

Table 3: Crustal heat flow value.

Stratigraphic age	Depth (m)	Thickness (m)	Heat generation rate ($\mu W/m^3$)	Heat flow value (mW/m^2)
Cenozoic	200.00	1562.41	0.122	190.6
Proterozoic	1762.41	318.07	0.044	14.0
Archaean	2080.48	375.92	0.75	281.94
Upper crust*	/	9000	1.24	11160
Middle crust*	/	7000	0.86	6020
Lower crust*	/	7000	0.31	2170

Note: representative data of "*" comes from Chang Jian (2016) [33].

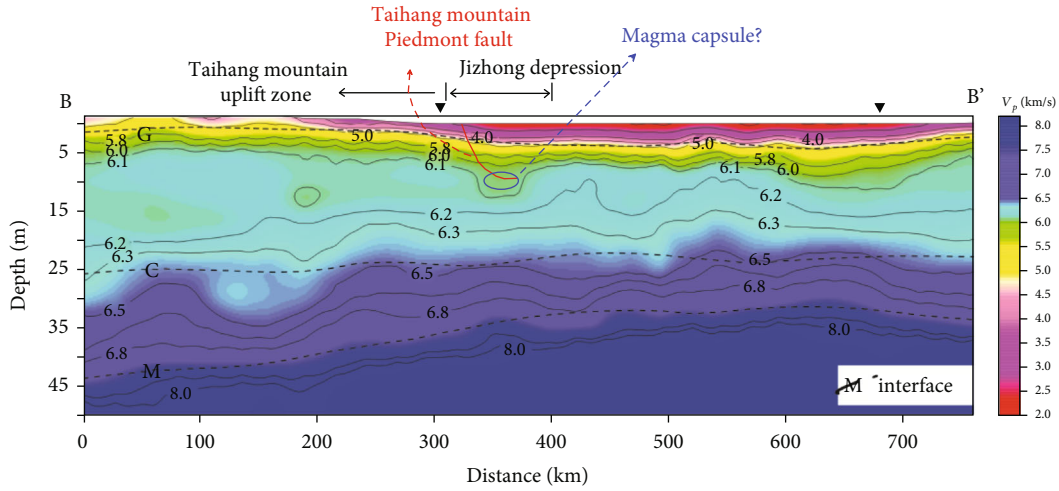

Figure 5: Velocity structure of profile BB′ (modified according to Duan et al. [24]).

fault, and there is no additional heat source such as magma capsule.

4.3. Heat Source Channel. There are two ways to transfer heat from the deep mantle to the crustal surface: one is to transfer heat through various rock strata by means of heat conduction; the other is to transfer the heat by means of thermal convection through deep faults with fluid as the carrier. The craton destruction in North China resulted in a huge thinning of the lithosphere in this area [42] that provided a good condition for the deep thermal energy entering the shallow strata [34]. According to the results of P wave velocity, regional crustal thickness is 32~35 km in Jizhong depression [43].

There are some secondary tectonic units in Jizhong depression, which is the secondary tectonic unit of North China basin. The fluid in the fault is convective due to the thermal potential difference, which brings the heat flow from the deep to the shallow. The mantle-derived helium found in the water of geothermal well indicates the intrusion of mantle-derived materials along the fault [44, 45]. The phenomenon of abnormally high soil radon content was also measured at the fault site in 2019 [43], which proved the existence of geothermal fluid convection to shallow strata indirectly.

Based on interpretations of magnetotelluric soundings (Figure 2), Niudong-Hexiwu fault that controls Niutuozhen uplift are detected. The main active period is often later than the second-order fault in the depression [46]. Other faults of magnetotelluric interpretation belong to small- and medium-sized faults with caprock properties, which occur in the Neogene. Deep geophysical survey result shows that Niudong-Hexiwu fault cuts the Moho surface that provides channels for geothermal fluids to enter the shallow layers, accompanied by thermal convection [47]. On February 12, 2018, the magnitude 4.3 earthquake occurred almost on the Niudong-Hexiwu fault, and the focal mechanism solution showed that seismogenic structure of the earthquake was the Niudong-Hexiwu fault, with right-lateral normal fault and focal depth 20 km [48]. This makes the Niudong-Hexiwu fault become an important channel of deep heat source in the region.

4.4. Heat Reservoir and Caprock. According to the electrical characteristics of MT profile, the changes of low-high or low-high-low-high in the profile are due to the differences in resistivity values of different lithologic strata, and the dense isoline region of resistivity symbolize the lithologic interface. Base on the logging data statistics of 7 Wells in Jizhong depression [49], the resistivity of Quaternary (Q) is about 20 Ω·m; the resistivities of sand and mudstone of Neogene (N) and Paleogene (E) are 3~9 Ω·m; the resistivities of Ordovician (O), Cambrian (ϵ), and Qingbaikou (Qn) are 200~300 Ω·m; the resistivity of carbonate rocks of Proterozoic Jixian (Jx) is about 1000 Ω·m. It can be seen that, among the strata at a certain depth in Jizhong depression, the

Table 4: Statistics of thermal conductivity of rock in JZ02.

Lithology	Sample quantity	Value range (W/mK)	Average value (W/mK)
Mudstone	9	1.45-2.45	2.01
Sandstone	8	1.99-3.59	2.48
Dolomite	8	2.70-5.41	4.53
Gneiss	12	2.10-3.24	2.58

resistivity of Jixian is the highest, followed by the Ordovician, Cambrian, and Qingbaikou, and the lowest is the Neogene and Paleogene. The carbonate rocks of Proterozoic Jixian are high resistivity layers that can be used as regional marker layers. Combined with the borehole data of JZ02, the geological structure profile (Figure 2) of Jizhong depression was compiled, which divided into five substructural units that include Daxing uplift, Langgu sag, Niutuozhen Uplift, Baxian depression, and Wen'an slope. Two secondary faults, named Xiadian fault and Niudong-Hexiwu fault, and a number of minor faults are identified. Xiadian fault and Niudong-Hexiwu fault control the two secondary structural units of Daxing uplift and Niutuozhen Uplift, respectively. It is the type of high convex for Daxing uplift [50]. The depth of the top of high resistivity carbonate rocks in the section is 1000~1800 m, and the thickness is about 1200 m, while the depth of the top of high resistance carbonate rock in Niutuozhen uplift is 1200~2700 m. The burial depth of the top of high resistance carbonate rocks in Langgu sag is greater than 5000 m. For Baxian sag, it is more than 6000 m.

The thermal conductivity of borehole cores is statistically analyzed (Table 4), and the results of 37 pieces are as follows:

(1) The average thermal conductivities of mudstone, sandstone, dolomite, and gneiss samples are 2.84 W/mK, ranging from 1.45 to 5.41 W/mK

(2) The thermal conductivity of mudstone is low, averaging 2.01 W/mK, between 1.45 and 2.45 W/mK; the second is sandstone, with an average thermal conductivity of 2.048 W/mK, between 1.99 and 3.59 W/mK; the average thermal conductivity of carbonate rocks (Dolomite) is 4.53 W/mK, between 2.70 and 5.41 W/mK

It can be seen that mudstone and sandstone with low thermal conductivity have poor ability of heat conduction. The Jixian carbonate rock of Proterozoic has a thermal conductivity far higher than that of other lithologic rocks, which is conducive to heat conduction in the carbonate reservoir. Figure 6 shows the thermal conductivity of strata at different depths. There are extremely thick mudstones and sandstones of Cenozoic interbedding in the study area, which can play a very good role in thermal insulation as the caprock. From the lithologic structure, the heat reservoir with high thermal conductivity and the cap layer with large thickness and low thermal conductivity are conducive to heat conduction and storage. In addition, in recent years, deep carbonate exploration in Jizhong depression found that

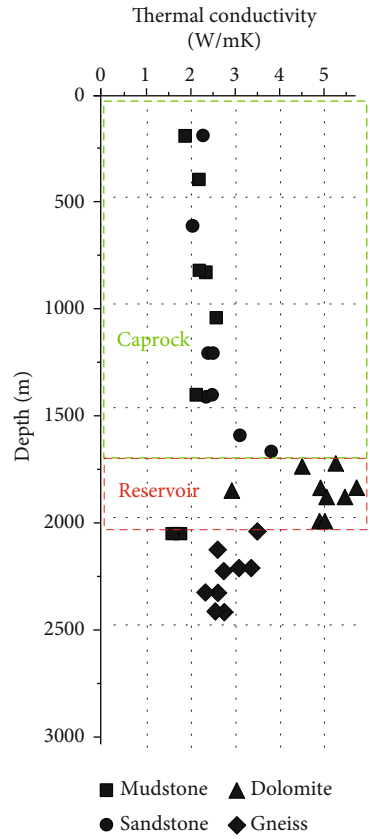

Figure 6: Scatter plot of thermal conductivity of rock for depths in JZ02.

there are thick cracks at the top of carbonate rocks, in which geothermal fluid has convection phenomenon [51], which is more conducive to the heat transmission in heat reservoir.

5. Conclusion

(1) From the perspective of heat source, the contribution of heat flow produced by radioactive heat generation in the crust is less than 30%. The layer with low velocity and high conductivity are caused by faults rather than magma capsule. Therefore, most of the heat source of geothermal reservoir comes from the mantle

(2) From the perspective of heat source channel, Niudong-Hexiwu fault is the regional deep fault that provide channel for deep heat convection to shallow stratums

(3) From the perspective of caprock and reservoir structure, geothermal exploitation is mostly located in the uplift area at the present stage, and the thermal reservoir with high thermal conductivity and the caprock with large thickness and low thermal conductivity are beneficial to the conduction and storage of heat. In addition, it was found that there are thick fissures at the top of carbonate rocks in recent years, in which

the geothermal fluid has convection phenomenon, which is more conducive to the spread of heat in the thermal reservoir

(4) In general, the main heat source in Jizhong depression comes from the mantle, which is transferred to the shallow stratum through heat conduction and heat convection. In the uplift area, due to the thick caprock with low thermal conductivity and the thermal reservoir with high thermal conductivity, it is beneficial to the accumulation of heat in the thermal reservoir

Data Availability

Some or all data, models, or code generated or used during the study are available from the corresponding author by request, such as (1) thermophysical parameters, (2) data of electromagnetic sounding, and (3) borehole lithology of JZ02.

Conflicts of Interest

The authors declare that they have no conflicts of interest.

Acknowledgments

This paper is funded by the Geological Survey Project of China Geological Survey (nos. DD20221676 and DD20190555).

References

[1] K. Y. Zheng and X. P. Pan, "Status and prospect of geothermal generation development in China," *Sino-Global Energy*, vol. 14, no. 2, pp. 45–48, 2009.

[2] G. B. Zhang, "Geothermal resource distribution and existing problems in exploitation and utilization," *Coal Geology of China*, vol. 18, no. 201, pp. 25–27, 2006.

[3] N. B. Li, J. W. Yang, Y. Yu, X. Li, and B. L. Ke, "Combination with development and innovation for efficient use of "two geothermal" in Beijing-Tianjin-Hebei economic zones," *Urban Geology*, vol. 12, no. 1, pp. 1–10, 2017.

[4] Z. Z. Zheng, "Study on the characteristics of hydrothermal geothermal resources," *Energy & Environment*, vol. 1, pp. 54-55, 2017.

[5] Z. Y. Zhou, S. L. Liu, and J. X. Liu, "Study on the characteristics and development strategies of geothermal resources in China," *Journal of Natural Resources*, vol. 30, no. 7, pp. 1210–1221, 2015.

[6] M. X. Chen, *Geothermal Resources in North China*, Science Press, Beijing, China, 1988.

[7] S. Feng and S. Hao, "Paleo temperature evolution and petroleum generation potential of Raoyang and Langgu subsidences of North China Basin," *Journal of the University of Petroleum*, vol. 25, no. 1, pp. 1–10, 1983.

[8] Y. L. Gong, L. S. Wang, S. W. Liu et al., "Distribution characteristics of terrestrial heat flow density in Jiyang depression of Shengli oilfield, East China," *China Science*, vol. 8, no. 4, pp. 384–391, 2003.

[9] S. H. Lin and Y. L. Gong, "Distribution characteristics of geotemperature field in Jizhong depression, North China," *Journal of East China Institute of Technology*, vol. 28, no. 4, pp. 359–364, 2005.

[10] R. X. Zhu, Y. G. Xu, G. Zhu, H. F. Zhang, Q. K. Xia, and T. Y. Zheng, "Destruction of the North China craton," *Science China Earth Sciences*, vol. 55, no. 10, pp. 1565–1587, 2012.

[11] X. Liu and G. Q. You, "Tectonic regional subdivision of China in the light of plate theory," *Geology in China*, vol. 42, no. 1, pp. 1–17, 2015.

[12] W. Huang, W. Gao, and G. Ding, "Neogene volcanism and Holocene earthquakes in the Tanlu fault zone, eastern China," *Tectonophysics*, vol. 260, no. 4, pp. 259–270, 1996.

[13] X. Z. Zhao, F. M. Jin, Q. Wang et al., "Buried-hill play, Jizhong subbasin, Bohai Bay basin: a review and future prospectivity," *AAPG Bulletin*, vol. 99, no. 1, pp. 1–26, 2015.

[14] L. Lin, S. M. Zhao, C. X. Ruan, and Y. P. Wang, "The inhomogeneity characteristics of geothermal storing karst caves of Wumishan reservoir of Jixian system in the deep part of Tianjin," *Geoscience*, vol. 21, no. 4, pp. 600–604, 2007.

[15] W. C. Zhang, D. Yang, Y. Chen, Z. Qian, and H. Liu, "Sedimentary structural characteristics and hydrocarbon distributed rules of Jizhong depression," *Acta Geologica Sinica*, vol. 82, no. 8, pp. 1103–1112, 2008.

[16] N. Yu and W. Pang, "Application of audiomagnetotelluric sounding in the geothermal exploration," *Hydrogeology & Engineering Geology*, vol. 37, no. 3, pp. 135–138, 2010.

[17] Q. Liu and Y. J. Gu, "Seismic imaging: from classical to adjoint tomography," *Tectonophysics*, vol. 566-567, pp. 31–66, 2012.

[18] K. Aki and W. Lee, "Determination of three-dimensional velocity anomalies under a seismic array using first P arrival times from local earthquakes: 1. a homogeneous initial model," *Journal of Geophysical Research*, vol. 81, no. 23, pp. 4381–4399, 1976.

[19] G. Laske and G. Masters, "Constraints on global phase velocity maps from long-period polarization data," *Journal of Geophysical Research: Solid Earth*, vol. 101, no. B7, pp. 16059–16075, 1996.

[20] V. Farra and R. Madariaga, "Non-linear reflection tomography," *Geophysical Journal of the Royal Astronomical Society*, vol. 95, no. 1, pp. 135–147, 1988.

[21] C. A. Zelt and D. J. White, "Crustal structure and tectonics of the southeastern Canadian cordillera," *Journal of Geophysical Research*, vol. 100, no. B12, pp. 24255–24273, 1995.

[22] C. A. Rychert, P. M. Shearer, and K. M. Fischer, "Scattered wave imaging of the lithosphere-asthenosphere boundary," *Lithos*, vol. 120, no. 1-2, pp. 173–185, 2010.

[23] J. W. Teng, Z. J. Zhang, X. K. Zhang et al., "Investigation of the Moho discontinuity beneath the Chinese mainland using deep seismic sounding profiles," *Tectonophysics*, vol. 609, pp. 202–216, 2013.

[24] Y. H. Duan, F. Y. Wang, X. K. Zhang et al., "Three-dimensional crustal velocity structure model of the middle-eastern north China Craton (HBCrust1.0)," *Science China Earth Sciences*, vol. 59, no. 7, pp. 1477–1488, 2016.

[25] N. S. Qiu, "Characters of thermal conductivity and radiogenic heat production rate in basins of Northwest China," *Scientia Geologica Sinica*, vol. 37, no. 2, pp. 196–206, 2002.

[26] Q. H. Guo, "Magma-heated geothermal systems and hydrogeochemical evidence of their occurrence," *Acta Geologica Sinica*, vol. 94, no. 12, pp. 3544–3554, 2020.

[27] Y. Zhang, J. B. Feng, Z. L. He, and P. W. Li, "Classification of geothermal systems and their formation key factors," *Earth Science Frontiers*, vol. 24, no. 3, pp. 190–198, 2017.

[28] A. G. E. Abbady and A. H. Al-Ghamdi, "Heat production rate from radioactive elements of granite rocks in north and south-eastern Arabian shield Kingdom of Saudi Arabia," *Journal of Radiation Research and Applied Sciences*, vol. 11, no. 4, pp. 281–290, 2018.

[29] X. G. Ou, Z. M. Jin, L. Wang, H. J. Xu, and S. Y. Jin, "Thermal conductivity and its anisotropy of rocks from the depth of 100-2000m mainhole of Chinese continental scientific drilling: revelations to the study on thermal structure of subduction zone," *Acta Petrologica Sinica*, vol. 20, no. 1, pp. 109–118, 2004.

[30] P. Zhao and J. Wang, "Characteristics of heat production distribution in SE China," *Acta Petrologica Sinica*, vol. 11, no. 3, pp. 292–305, 1995.

[31] F. Birch, R. F. Roy, and E. R. Decker, "Heat flow and thermal history in, New York and New England," in *Studies of Appalachian Geology: Northern and Maritime*, E. Zen, W. S. White, J. B. Hadley, and J. B. Thompson Jr., Eds., pp. 437–451, Interscience, New York, NY, USA, 1968.

[32] J. Y. Wang and J. A. Wang, "Mantle heat flow of Liaohe rifted basin in North China," *Acta Geophysica Sinica*, vol. 29, no. 5, pp. 450–458, 1986.

[33] J. Chang, N. Qiu, and X. Zhao, "Present-day geothermal regime of the Jizhong depression in Bohai bay basin, East China," *Chinese Journal of Geophysics-Chinese Edition*, vol. 59, no. 3, pp. 1003–1016, 2016.

[34] G. L. Wang, W. Zhang, W. J. Lin et al., "Research on formation mode and development potential of geothermal resources in Beijing-Tianjin-Hebei region," *Geology in China*, vol. 44, no. 6, pp. 1074–1085, 2017.

[35] M. Salah and D. Zhao, "3-D seismic structure of Kii Peninsula in southwest Japan: evidence for slab dehydration in the forearc," *Tectonophysics*, vol. 364, no. 3-4, pp. 191–213, 2003.

[36] H. J. Müller and S. Raab, "Elastic wave velocities of granite at experimental simulated partial melting conditions," *Physics & Chemistry of the Earth*, vol. 22, no. 1-2, pp. 93–96, 1997.

[37] Y. S. Zhou and C. R. He, "The relationship between low velocity layers and rheology of the crust in North China and its effect on strong earthquake," *Seismology and Geology*, vol. 24, no. 1, pp. 124–132, 2002.

[38] Z. H. Luo, "Fluid earth science and earth system science," *Earth Science Frontiers*, vol. 25, no. 6, pp. 283–288, 2018.

[39] S. Jin, W. B. Wei, S. Wang, G. F. Ye, and H. D. Tan, "Discussion of the formation and dynamic signification of the high conductive layer in Tibetan crust," *Chinese Journal of Geophysics-Chinese Edition*, vol. 53, no. 10, pp. 2376–2385, 2010.

[40] N. I. Christensen and W. D. Mooney, "Seismic velocity structure and composition of the continental crust: a global view," *Journal Geophysics Research*, vol. 100, no. B6, pp. 9761–9788, 1995.

[41] S. B. Smithson, F. Wenzel, Y. V. Ganchin, and I. B. Morozov, "Seismic results at Kola and KTB deep scientific boreholes: velocities, reflections, fluids, and crustal composition," *Tectonophysics*, vol. 329, no. 1-4, pp. 301–317, 2000.

[42] F. Y. Wu, Y. G. Xu, S. Gao, and J. P. Zheng, "Lithospheric thinning and destruction of the North China craton," *Acta Petrologica Sinica*, vol. 24, no. 6, pp. 1145–1174, 2008.

[43] Q. Z. Miao, G. L. Wang, S. H. Qi, L. X. Xing, H. L. Xin, and X. N. Zhou, "Genetic mechanism of geothermal anomaly in the Gaoyang uplift of the Jizhong depression," *Frontiers in Earth Science*, vol. 10, article 88519, no. 10, 2022.

[44] P. G. Burnard, R. Hu, G. Turner, and X. Bi, "Mantle, crustal and atmospheric noble gases in Ailaoshan gold deposits, Yunnan Province, China," *Geochimica et Cosmochimica Acta*, vol. 63, no. 10, pp. 1595–1604, 1999.

[45] Q. Y. Yang, Q. J. Wu, Y. R. Sheng, J. Song, and L. Di, "Regional seismic body wave tomography and deep seismogenic environment beneath Zhangbo seismic belt and its adjacent area," *Chinese Journal of Geophysics*, vol. 33, no. 8, pp. 3251–3262, 2018.

[46] C. A. Zhou, X. P. Li, W. J. Xin et al., "Research on hydrocarbon accumulating conditions of internal buried hills exploration in Niutuozhen uplift in Jizhong sag," *China Petroleum Exploration*, vol. 15, no. 2, pp. 29–32, 2010.

[47] C. Y. Wang, Y. H. Duan, and Q. J. Wu, "Exploration on the deep tectonic environment of strong earthquakes in North China and relevant research findings," *Acta Seismologica Sinica*, vol. 38, no. 4, pp. 511–516, 2016.

[48] H. Li, Y. B. Dong, and Y. X. Wang, "Seismological evidence for a deep-seated shear zone in the Langgu depression," *Chinese Journal of Geophysics*, vol. 63, no. 2, pp. 492–504, 2020.

[49] Z. Shi, H. Zhang, T. Duan, and P. Zhang, "Investigation of oil and gas reservoir in Jizhong depression based on time-frequency electromagnetic method," *Global Geology*, vol. 37, no. 2, pp. 585–594, 2018.

[50] M. X. Chen and J. Y. Wang, "The characteristics of the geothermal field and its formation mechanism in the North China Down-Faulted Basin," *Acta Geologica Sinica*, vol. 64, no. 1, pp. 80–91, 1990.

[51] G. L. Wang, J. Gao, B. J. Zhang, Y. F. Xing, W. Zhang, and F. Ma, "Study on the thermal storage characteristics of the Wumishan formation and huge capacity geothermal well parameters in the Gaoyang low uplift area of Xiong'an new area," *Acta Geologica Sinica*, vol. 94, no. 7, pp. 1970–1980, 2020.